

Excitation of surface plasmons on metals by low-energy electrons: The role of interference effects

Burl M. Hall and D. L. Mills

Department of Physics, University of California, Irvine, California 92717

(Received 19 December 1990; revised manuscript received 25 February 1991)

We present quantitative theoretical studies of the wave-vector dependence of the cross section for excitation of surface plasmons by low-energy electrons incident on the Ag(100) surface. The analysis assumes the dipole mechanism provides the dominant coupling between the electron and the surface plasmon. The theory provides a very good account of the systematic features reported recently by Rocca and Valbusa. As emphasized in earlier theoretical discussions, under conditions used in the experiments, the interference between two excitation channels—"loss then reflection" and "reflection then loss"—enters importantly in the description of the excitation process. In addition, it is essential to include the influence of the image potential on both the amplitude and phase on the scattering amplitude for elastic, specular reflection from the surface.

I. INTRODUCTION

Currently there is great interest in the use of electron-energy-loss spectroscopy to study the dispersion relation of surface plasmons on a variety of simple metal surfaces.¹⁻⁵ As a result of these studies, quantitative data on the surface-plasmon dispersion are now in hand, for several surfaces. Most intriguing also is the experimental discovery of certain surface modes of multipole character,³ which had been predicted some years ago in theoretical studies by Eguluz and Quinn.⁶

It is in fact the case that the surface-plasmon dispersion on Al(111) was studied many years ago by Porteus and Faith,⁷ by the electron-energy-loss method. The rather broad loss peaks reported in these early studies proved difficult to interpret unambiguously.^{8,9} The structures reported in the new generation of experiments are quite sharp, and thus provide direct and unambiguous information on surface-plasmon dispersion.

In their studies of surface plasmons on Ag(100) by electron-energy-loss spectroscopy, Rocca and his collaborators also examined the variation of the excitation cross section with wave vector, in the near-specular geometry, to find a rather complex behavior that depended on beam energy and scattering geometry.^{4,5} The cross section did not exhibit a maximum when the surface-plasmon wave vector Q_{\parallel} vanishes, as elementary considerations might suggest should happen. These authors argued (correctly as we shall see) that interference effects in the matrix element which controls the excitation process are responsible for the complex behavior of the cross section. The electron may excite the surface plasmon on the incoming portion of its trajectory, then back reflect off the surface at the scattered energy, or it may reflect first at the incident energy, then excite the surface plasmon on the exit portion of its trajectory. The authors of Ref. 4 argued that such interference effects have yet to be incorporated into the theory of surface-plasmon excitation, and suggested a modified version of a formula derived by Persson¹⁰ in another context might prove suitable for the purpose.

It is the case, however, that a rather general theory of electron energy loss in the backscattering geometry was formulated a number of years ago,¹¹ with explicit application to electronic excitations at surfaces, including surface plasmons. The theory applies to the case where the excitation process involves a small angle deflection, and the dipole mechanism is dominant. The interference effect discussed by Rocca and collaborators is incorporated fully in the theory, and the potential importance of these effects under conditions realized in their experiments was noted and discussed quite explicitly.¹² The interference effect is included also in earlier discussions of dipole scattering from surface vibrations,¹³ though in general the interference effects play a minor role in the excitation of vibrational losses; this is because the energy transfer and angular deflections are quite small. However, we note the very interesting discussion given by Froitzheim and Kohler, of their influence on the cross section for exciting the CO stretching vibration, on the Ni(111) surface.¹⁴ Also when beam energies in the near vicinity of fine-structure resonances are employed, the issue arises once again, as discussed some years ago¹⁵ in the analysis of excitation of vibrational modes of hydrogen adsorbed on W(100), in the impact scattering regime.

It is also the case, however, that the theory, with full incorporation of the interference effects just discussed, has never been compared with experimental data in a detailed manner, under conditions where the interference affects the excitation cross section importantly. One requires as input the complex scattering *amplitudes* (not intensities) which describe the elastic reflection of the electron off the surface, at both the incident energy and angle, and also for that associated with the trajectory of the scattered electron. Intensities for the elastic scattering from the surface [low-energy electron diffraction (LEED) intensities] must be available to serve as a guide, in addition to the inelastic cross-section data, before an analysis can be made with confidence.

The very interesting data reported by Rocca and co-workers allow us the opportunity to address this question now. They report, as noted earlier, the wave-vector

dependence of the cross section for exciting surface plasmons. In addition, they have measured the energy variation of the elastic scattering intensity of the specular beam at three angles of incidence, in the energy regime used in the surface-plasmon studies. At the low impact energies employed in this work (and which are employed in most studies of surface-plasmon excitation by low-energy electrons), the image potential influences the elastic scattering intensities importantly. Indeed, fine-structure resonances are evident in the data.⁵ We have, however, enough information in hand to construct an adequate model of the image barrier for Ag(100), from these data. Through use of this image barrier, in combination with a multiple scattering calculation of the elastic scattering amplitudes, we can explore the theoretical predictions for the wave-vector dependence of the surface-plasmon cross section. We have achieved a very good account of the data in this manner.

The outline of this paper is as follows. In Sec. II we review the theory of surface-plasmon excitation in the dipole regime, with attention to casting the results into a form that can be placed alongside the data on Ag(100). Also, while we have no adjustable parameters in our calculation of the surface-plasmon cross section (once we have chosen an image barrier that accounts for the elastic scattering data), there are approximations we invoke, and we discuss these in Sec. II. Section III is devoted to analysis of the low-energy electron diffraction data, and our image barrier, while the final results are presented and discussed in Sec. IV.

II. GENERAL COMMENTS

In this section, we review the basic theory of electron energy loss by means of the dipole mechanism, as discussed in Ref. 11.

The discussion begins by considering any elementary excitation (surface plasmon, particle-hole pair, nuclear motions associated with lattice vibrations) which produces a fluctuation $\delta\rho(\mathbf{r},t)$ in charge density within the substrate, with the form $\delta\rho(r,t) = \delta\rho_{Q_{\parallel}}(z)\exp(i\mathbf{Q}_{\parallel}\cdot\mathbf{r}_{\parallel} - i\omega t)$, where z is normal to the surface, and the subscript \parallel refers to either a vector which lies in the x - y plane, or the projection of a vector onto the x - y plane. It is assumed $|\mathbf{Q}_{\parallel}|$ is small, in the sense that $|\mathbf{Q}_{\parallel}|a_0 \ll 1$ with a_0 a lattice constant or microscopic length characteristic of the substrate, and that $\delta\rho_{Q_{\parallel}}(z)$ varies slowly with z , on this length scale. Small values of $|\mathbf{Q}_{\parallel}|$ are encountered in the near-specular energy-loss studies of interest here.

Such a charge fluctuation produces a long-range electric field outside the crystal, in the vacuum above it. If $\phi(\mathbf{r},t)$ is the electrostatic potential from which this field is calculated, the fact that the dependence of $\phi(\mathbf{r},t)$ with \mathbf{r}_{\parallel}

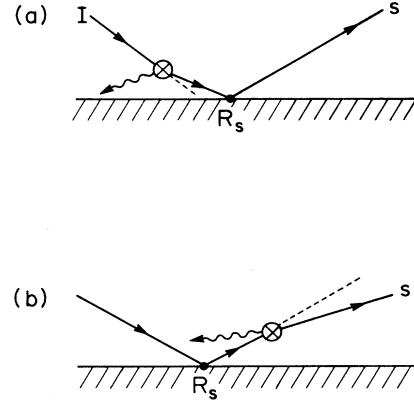


FIG. 1. A schematic illustration of the two excitation processes incorporated into the theory of the excitation of surface plasmons by the dipole mechanism. We have (a) excitation of the surface plasmon on the incoming leg of the trajectory, and (b) excitation on the outgoing leg.

must be of the form $\exp(i\mathbf{Q}_{\parallel}\cdot\mathbf{r}_{\parallel})$, and the requirement $\nabla^2\phi=0$ outside the crystal, lead to the form $\phi(\mathbf{r},t) = \phi_{Q_{\parallel}}\exp(i\mathbf{Q}_{\parallel}\cdot\mathbf{r}_{\parallel} - Q_{\parallel}z - i\omega t)$. Thus, when \mathbf{Q}_{\parallel} is small, the potential extends far into the vacuum above the substrate.

The electron scatters inelastically from the electric field above the crystal, in this picture. It may do so as it approaches the crystal, as depicted in Fig. 1(a), or as it exits, as depicted in Fig. 1(b). One calculates the contribution from each leg to the excitation matrix element, and adds them before squaring to form the total cross section.¹¹ They then interfere, and the central question explored in this paper is the influence of the interference effects, with emphasis on the situation where the complex amplitudes for elastic reflection from the surface, R_I and R_s , differ substantially.

The electron penetrates into the crystal a bit, of course, and will interact with the surface plasmon while inside the crystal. As noted in a review article some years ago,¹⁶ when coupling of the electron to the surface plasmon while inside the crystal enters the excitation matrix element importantly, one expects to see the bulk-plasmon line in the loss spectrum, in addition to the surface plasmon. Such a bulk-plasmon loss appears in the early work of Proteus and Faith,⁷ on Al(111). In the experiments which motivated the present analysis, there is no hint of the bulk-plasmon loss.¹⁷ We shall then assume that the dipole excitation model described above applies in this instance.

The theory gives the scattering efficiency S per unit solid angle, per unit energy, which we write here as $d^2S/d\Omega(\hat{k}_s)dE$. One has¹¹

$$\frac{d^2S}{d\Omega(\hat{k}_s)dE} = \frac{e^2 m^2 v_{\parallel}^2}{\pi^2 \hbar^4 \cos\theta_I} \left[\frac{k_s}{k_I} \right] \frac{1}{Q_{\parallel}} \left[\frac{|v_{\parallel} Q_{\parallel} (R_s + R_I) + i(R_I - R_s)(\omega - \mathbf{v}_{\parallel} \cdot \mathbf{Q}_{\parallel})|^2}{[v_{\parallel}^2 Q_{\parallel}^2 + (\omega - \mathbf{v}_{\parallel} \cdot \mathbf{Q}_{\parallel})^2]^2} \right] \text{Im} \left[\frac{-1}{1 + \epsilon(\omega)} \right]. \quad (2.1)$$

In this expression, the energy loss is $\hbar\omega$. The quantities v_{\perp} and v_{\parallel} are the velocities normal and parallel to the surface for the incoming electron, k_s and k_I the wave vectors of the scattered and incident electrons, and θ_I the angle of incidence. Once again, R_I and R_s are the reflection amplitudes; the intensity of the specular beam at the incident energy is $|R_I|^2$. Finally $\epsilon(\omega)$ is the complex dielectric constant of the substrate.

For a material such as a simple metal that supports a surface plasmon, $\text{Im}\{-1/[1+\epsilon(\omega)]\}$ has a peak at the long-wavelength surface-plasmon frequency ω_s , for which $\text{Re}[\epsilon(\omega_s)] = -1$. The simple theory of Ref. 11 does not provide an account of the influence of the wave-vector dependence of the surface-plasmon frequency on the loss spectrum. Our interest is in the matrix element for excitation of the wave, and its dependence on Q_{\parallel} . This is contained in the prefactor of $\text{Im}\{-1/[1+\epsilon(\omega)]\}$ in Eq. (2.1), and is affected little by the small (but very interesting) frequency shifts introduced by dispersion.

Early theories of dipole excitation of surface modes employ a classical trajectory analysis of the excitation event.¹⁸ When the physical content of such a calculation is translated into the language of quantum mechanics, such calculations assume $R_s = R_I = 1$, which is surely unphysical for any real material. In this limit, as discussed earlier,^{11,13,16} Eq. (2.1) reproduces the results of the classical trajectory analysis. For small energy vibrational losses, one may assume usually $R_s \cong R_I$, and one then sees the excitation cross section assumes the form provided by classical trajectory analysis, except the excitation

probability provided by this theory is multiplied by $|R_I|^2$, a factor which dramatically reduces the loss probability, and introduces additional energy dependence. When $R_I \neq R_s$, as in the experiments of interest here, the full quantum-mechanical treatment of Ref. 11 must be used.

The experiments of Rocca, Biggio, and Valbusa do not probe the scattering efficiency per unit solid angle displayed in Eq. (2.1). In the experiment, the entrance slits of the detector are long, narrow slits oriented normal to the scattering plane,¹⁷ which we assume to be the x - z plane. The slits subtend an angle $\Delta\theta_s$ of roughly 2° . We thus form a scattering efficiency ($d^2S/d\theta_s dE$) by integrating Eq. (2.1) over the momentum transfer Q_y normal to the scattering plane, noting the relation¹³ $dQ_x dQ_y = d\Omega(\hat{k}_s)k_s^2 \cos\theta_s$. Hence

$$\frac{d^2S}{d\theta_s dE} = \left[\frac{dQ_x}{d\theta_s} \right] \int_{-\infty}^{+\infty} \frac{dQ_y}{k_s^2 \cos\theta_s} \frac{d^2S}{d\Omega(\hat{k}_s) dE}, \quad (2.2)$$

where also $dQ_x/d\theta_s = k_s \cos\theta_s$.

One may evaluate the integral in Eq. (2.2) analytically, provided we treat R_s as a constant. We do so by evaluating R_s for a scattered trajectory which lies in the scattering plane. This is a distinct approximation, particularly in energy regimes where there is structure in the reflectivity. However, it would be most difficult to proceed without invoking this step.

If we define $\bar{R} = (R_I + R_s)/2$, and also let $\Delta = (R_I - R_s)/(R_I + R_s)$, one has

$$\begin{aligned} \frac{d^2S}{d\theta_s dE} = & \frac{e^2 m^2 v_{\perp}^2}{\pi^2 \hbar^4 k_I \cos\theta_I} \text{Im} \left[\frac{-1}{1+\epsilon(\omega)} \right] \\ & \times \left[\frac{4|\bar{R}|^2}{v_{\perp}^2 Q_x^2 + (\omega - v_{\parallel} Q_x)^2} \left(1 + \frac{v_{\perp}^2 Q_x^2 \ln[F(Q_x)]}{|\omega - v_{\parallel} Q_x| [v_{\perp}^2 Q_x^2 + (\omega - v_{\parallel} Q_x)^2]} \right) + \frac{2\pi i |\bar{R}|^2 (\Delta - \Delta^*) (\omega - v_{\parallel} Q_x)}{[v_{\perp}^2 Q_x^2 + (\omega - v_{\parallel} Q_x)^2]^{3/2}} \right. \\ & \left. + \frac{|R_s - R_I|^2}{v_{\perp}^2 Q_x^2 + (\omega - v_{\parallel} Q_x)^2} \left[\frac{v_{\perp}^2 Q_x^2 + 2(\omega - v_{\parallel} Q_x)^2}{|\omega - v_{\parallel} Q_x| [v_{\perp}^2 Q_x^2 + (\omega - v_{\parallel} Q_x)^2]^{1/2}} \ln[F(Q_x)] - 1 \right] \right] \end{aligned} \quad (2.3a)$$

where

$$F(Q_x) = \frac{1}{v_{\perp} |Q_x|} \{ |\omega - v_{\parallel} Q_x| + [v_{\perp}^2 Q_x^2 + (\omega - v_{\parallel} Q_x)^2]^{1/2} \}. \quad (2.3b)$$

The last term in Eq. (2.3a) has a weak logarithmic singularity as $Q_x \rightarrow 0$. In fact, as mentioned earlier, in the experiment, the detector samples a range of Q_x values, corresponding to $\Delta\theta_s \sim 2^\circ$. In our numerical work, we simulate the effect of averaging over a range of Q_x by replacing $|Q_x|$ in Eq. (2.3b) by $(Q_x^2 + Q_c^2)^{1/2}$, with Q_c chosen equal to the value of ΔQ_x that would correspond to a spread in scattering angle of 2° . Since the singularity is in the logarithm, our final results are rather insensitive to the means we use to simulate the averaging over Q_x .

There is one final issue. The kinematical prefactors in the basic expression for the plasmon excitation cross section in Eq. (2.1) [the factor in large parentheses, which appears in front of Eq. (2.1)] are calculated under the assumption that the electron wave function in the vacuum above the crystal is well approximated by a plane wave, unmodified by the image potential. It is a rather involved matter to improve this expression, and we retain the form in Eq. (2.1) in what follows.

We have reviewed the content of the dipole theory of surface-plasmon excitation here, along with its limitations so the reader can appreciate that there are indeed approximations in the expression used for the calculations reported below. For this reason, we can expect some discrepancies between theory and experiment, although on the whole we will find the agreement to be quite satisfactory. As remarked earlier, once we adjust

the barrier so the elastic reflectivity data is reproduced to our satisfaction, there are no adjustable parameters in our calculation of the surface-plasmon cross section.

III. THE ELASTIC SCATTERING AMPLITUDES

In order to proceed further, we need to know R_I and R_s . To generate these, we use the standard multiple scattering theory for low-energy electron diffraction, as presented by Van Hove and Tong.¹⁹ The procedure is to use phase shifts calculated from a self-consistently generated band-structure potential to obtain the single-site t matrix that describes the scattering from a single atom embedded in the substrate. In the present work, we employed the phase shifts for the Ag potential generated by Jepsen and co-workers.²⁰ The single-site t matrix is then used to calculate layer diffraction matrices for a single layer of Ag atoms.

Because of the two-dimensional periodicity of each layer, an electron with wave vector \mathbf{k}_I incident on a plane of Ag atoms can scatter elastically only into a finite number of directions, which are determined by conservation of wave-vector components parallel to the surface. If the subscript \parallel denotes the projection of a vector onto a plane parallel to the surface, or a vector which lies within this plane, then $\mathbf{k}_{F\parallel} = \mathbf{k}_{I\parallel} + \mathbf{g}_{\parallel}$, where \mathbf{g}_{\parallel} is a surface reciprocal lattice vector. Thus, all possible scatterings off a single silver layer can be described by a matrix linking the incident wave with the various scattered waves. To calculate the reflection amplitude of the whole crystal, one needs to stack the layers to form the crystal, and sum over all possible scatterings. We have proceeded here by using the renormalized forward scattering (RFS) method developed by Pendry²¹ to combine the diffraction matrices for each layer, to form the total amplitude of the beams reflected from the crystal.

Standard LEED calculations, designed to apply to beam energies in excess of 50 or 100 eV, contain an important approximation that works very poorly at the low beam energies of interest here. One assumes that the potential at the interface between the crystal and the vacuum is a simple step, from the vacuum to an inner potential appropriate to the substrate. Moreover, one assumes the electron wave diffracts across the step without reflection. In the present case, where beam energies are in the 10–20-eV image, we require a description of the influence of the image potential on the reflection amplitudes R_I and R_s , and we must match the wave function and its derivative properly at the surface.

Far from the crystal, the image potential must have the form $-e^2/(4|z - z_0|)$, where z_0 is the location of the image plane, and z is normal to the surface. Closer in, exchange and correlation effects introduce terms which vary initially²² as $1/|z - z_0|^2$. There is no full microscopic theory of how the image potential joins onto the inner potential, so we must resort to a model. We use that proposed by Malström and Rundgren.²³ A cubic polynomial is employed to connect the inner potential to the asymptotic form far from the crystal. The image potential has both a real and imaginary part, given by

$$\operatorname{Re}[V(z)] = \begin{cases} -V_0, & z \geq 0 \\ \sum_{n=0}^3 a_n z^n, & z_1 \leq z \leq 0 \\ -\frac{e^2}{4|z - z_0|} = \frac{V_1}{|z - z_0|^2}, & z \leq z_1, \end{cases} \quad (3.1a)$$

$$\operatorname{Im}[V(z)] = \begin{cases} -V_I, & z \geq 0 \\ \sum_{n=0}^3 b_n z^n, & z \leq z \leq 0 \\ -\frac{V_2}{|z - z_0|^2}, & z = z_1. \end{cases} \quad (3.1b)$$

The crystal is in the upper half space, clearly, and $z_1 < z_0 < 0$. Inside the crystal, the inner potential has a real part V_0 and an imaginary part V_I . The coefficients of the two cubic polynomials are constrained to make the potential and its first derivative constant at $z=0$, and also at the matching point z_1 . We then use this form to calculate R_I and R_s , with, of course, multiple scattering from the ion cores incorporated when the electron is in the crystal. We can incorporate the influence of the image potential into the multiple scattering analysis by introducing appropriate reflection matrices from it; these are diagonal in the wave-vector representation outlined earlier, since the image potential depends only on z .

If $E_z = E - \hbar^2(\mathbf{k}_{\parallel} + \mathbf{g}_{\parallel})^2/2m$, for the energies of interest, we need to integrate the Schrödinger equation

$$\frac{d^2\psi}{dz^2} + \frac{2m}{\hbar^2}[E_z - V(z)]\psi = 0 \quad (3.2)$$

from $z=0$ to $z=z_1$, in the course of constructing the reflection matrices. This is done numerically. For $z < z_1$, the solution of the Schrödinger equation may be described by Whittaker functions. Through matching of the numerically generated function and its derivative at $z=z_1$ to the Whittaker functions, we can construct the reflection and transmission matrices for the image barrier, and then incorporate these into appropriate modifications of the RFS routines. In this scheme, the image barrier is treated formally as an additional layer added to the semi-infinite crystal.

One must determine the free parameters in the model by fitting data on the variation with energy or angle of the various LEED beams. Here, we examine the energy variation of the specular beam for three angles of incidence, 73.15° off the normal, 60° off the normal, and 49.3° off the normal. As a starting point, we chose the various parameters to be the same as those found earlier to give good agreement with data on Cu(100).²⁴ These parameters were $z_0 = -0.3 \text{ \AA}$, $z_1 = -2.0 \text{ \AA}$, $V_1 = 1.0 \text{ eV \AA}^2$, $V_2 = 1.5 \text{ eV \AA}^2$, $V_0 = 11 \text{ eV}$, and $V_I = 1.0 \text{ eV}$, where the origin of the coordinate system is half the nearest-neighbor distance above the outermost layer of Cu nuclei. This is a reasonable starting point, since Cu lies directly above Ag in the Periodic Table.

This set of parameters, when applied to Ag with the same convention used to locate $z=0$ (half the nearest-neighbor Ag distance) gave rather poor agreement with the data. In particular, the large peak about 1 eV below the beam emergence threshold was found to be too low in energy. This implies we must choose parameters that make the image potential well narrower, an effect that moves the resonance responsible for this peak upward in energy.²⁵ After a search, we found reasonable agreement with experiment with the choice $z_0 = -0.01 \text{ \AA}$, $z_1 = -2.5 \text{ \AA eV \AA}^2$, $V_2 = 1.5 \text{ eV \AA}^2$, $V_0 = 11 \text{ eV}$, and $V_I = 1.0 \text{ eV}$. We did not optimize the fit to the data, but simply searched for a parameter set that reproduced the principal features in the data reasonably well.

In Figs. 2–4, we see a comparison between theory and experiment for the intensity of the specular beam as a function beam energy, for the three angles of incidence. In Fig. 2, the data are similar to those in Fig. 7 of the paper by Rocca, Biggio, and Valbusa, but these are newer data provided also by Rocca and Valbusa. The data in Figs. 3 and 4 were kindly provided by Rocca.¹⁷ In all three figures, the data are presented as squares. The dashed lines are the results of theoretical calculations which ignore the influence of the image potential. The solid lines are the reflection coefficients calculated from the theory, with the image potential described by the parameters given above.

In Figs. 3 and 4, we have a direct comparison between theory and experiment, with the theory “calibrated” with one multiplicative parameter that produces roughly the right height for the prominent image potential generated resonance just below 10 eV. Note that while we find the reflectivity rather insensitive to energy above 10.5 eV, a property evident in the data, in fact the experimental reflectivity is really very small (essentially zero) in this re-

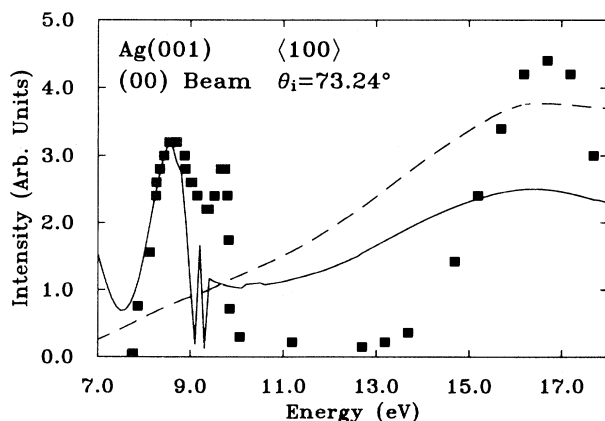


FIG. 2. Comparison between theory and experiment, for the LEED specular beam, for the case where the angle of incidence is 73.15° . The solid line is the calculation using the model barrier described in the text, with “background subtraction” from the theory as discussed in Sec. III. The dashed line is the specular intensity calculated with no image barrier. The squares are the data provided by Rocca.

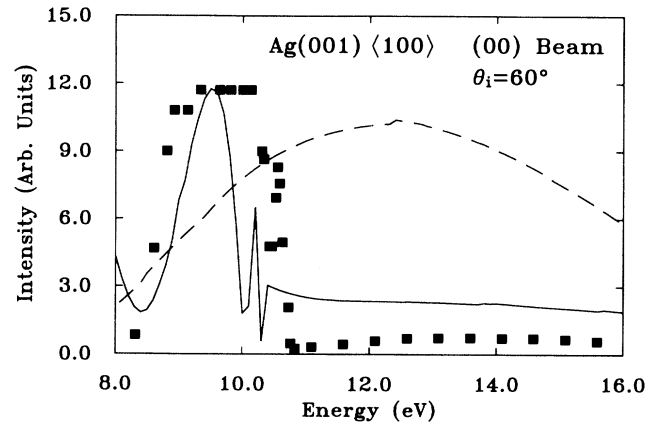


FIG. 3. The same as Fig. 2, except the angle of incidence is 60° . There is no “background subtraction” from the theory. The data have been kindly supplied by Rocca.

gion. We believe this aspect of the data is open to question, and may be the consequence of overestimating the background. When we compared theory with the data for $\theta = 73.15^\circ$, we found the theoretical energy variations to lie on top of a “background” not evident in the data. We were not able to get the theoretical reflectivity to be as small near 10–11 eV (relative to the major peak) as reported in Ref. 5. We have thus subtracted a “background” of roughly 0.07, in the units of Fig. 2, from the theoretical curve, when we compare with experiment. Part of this problem, of course, may have its origin in the fact that the model barrier has not been fully optimized. The surface-plasmon cross sections reported below are calculated with the full theoretical reflection amplitudes provided by theory, it should be remarked.

It is also the case that the theory places the emergence threshold for the $(\bar{1}\bar{1})$ beam about 0.4 eV below that

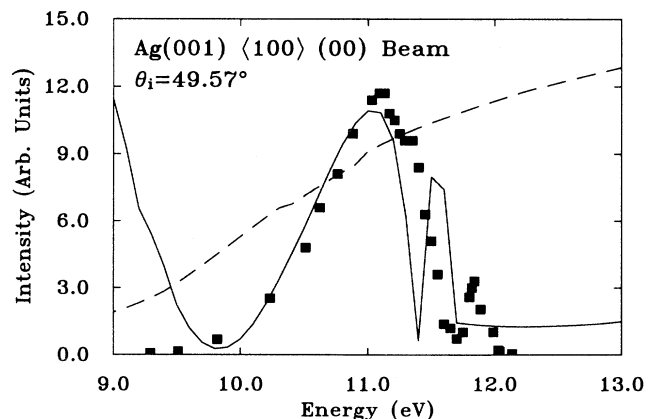


FIG. 4. The same as Fig. 2, except the angle of incidence is 49.3° . There is no “background subtraction” from the theory. The data have been kindly supplied by Rocca.

found in the data, to judge from the structures in the specular intensities induced at beam emergence. This has little to do with our particular model of the image barrier, note, since the beam emergence energy is given by a simple kinematical consideration. Such discrepancies have been noted before, and discussed by McRae.²⁶ So far as we know, they are not understood. A shift of the theoretical curve in Fig. 2 upward by 0.4 eV noticeably improves the agreement between theory and experiment.

Clearly, the model image barrier we have used accounts for the principal features in the data, though agreement between theory and experiment is not perfect. We regard the comparison as adequate, and we now examine the wave-vector dependence of the surface-plasmon cross section produced by this picture.

IV. THE WAVE-VECTOR DEPENDENCE OF THE SURFACE-PLASMON CROSS SECTION

In Figs. 5 and 6, we display our calculations of the dependence of the surface-plasmon cross section on wave vector Q_{\parallel} , for the three scattering configurations discussed in Refs. 4 and 5. In Fig. 7, we reproduce the data given as Fig. 3(a) in the paper by Rocca and Valbusa.⁴ The results in Fig. 5 are calculated with R_s and R_I generated without the image barrier, and Fig. 6 incorporates its influence. We see the two results differ quite dramatically. The parameter Q_c which enters the discussion which follows Eqs. (2.3) has been set to the value 0.05 \AA^{-1} , and we use the experimentally measured surface-plasmon frequency $\omega(Q_{\parallel})$ for each Q_{\parallel} in the determination of the scattered electron energy, and in the prefactor in Eqs. (2.3). Also v_{\parallel} and v_{\perp} in these expressions have been replaced by the average of the incident and scattered electron velocities, evaluated in the scattering plane.

These results are to be compared with the data of Roc-

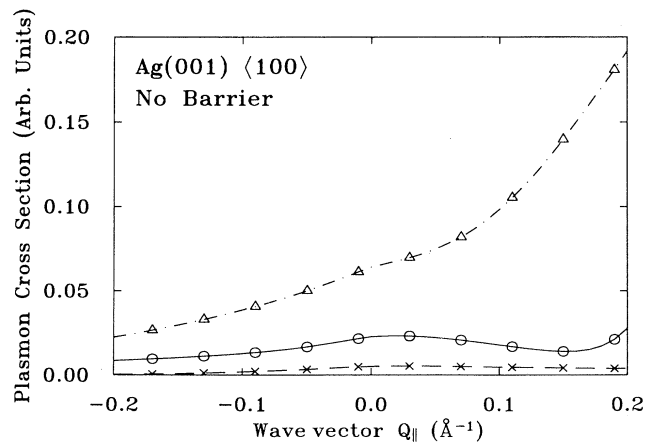


FIG. 5. Theoretical calculations of the surface-plasmon excitation cross section, with R_I and R_s calculated without use of the image barrier. The triangles are for a beam energy $E_I = 10.5 \text{ eV}$, and scattering angle $\theta_s = 86.2^\circ$, the \times 's $E_I = 16 \text{ eV}$ and $\theta_s = 60^\circ$, and the circles for $E_I = 16 \text{ eV}$ and $\theta_s = 81.6^\circ$.

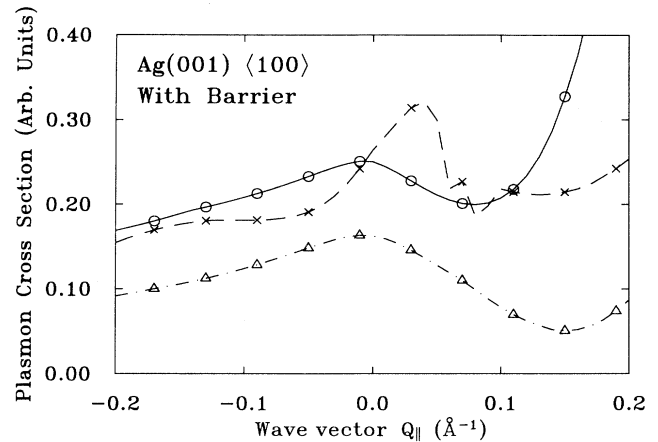


FIG. 6. Theoretical calculations of the surface-plasmon excitation cross section, for the case where R_I and R_s are influenced by the image barrier. The triangles are for a beam energy $E_I = 10.5 \text{ eV}$, and the scattering angle $\theta_s = 86.2^\circ$. The \times 's correspond to $E_I = 16 \text{ eV}$ and $\theta_s = 60^\circ$, and the circles $E_I = 16 \text{ eV}$ and $\theta_s = 81.6^\circ$.

ca and Valbusa, reproduced as our Fig. 7. We have used the same conventions in plotting our theoretical results found in Ref. 4. Thus the circles are calculated for the case where $E_I = 16 \text{ eV}$, and the scattered angle is 81.6° , the \times 's are for $E_I = 16 \text{ eV}$ and a scattered angle of 60° , and the triangles for $E_I = 10.5 \text{ eV}$ and a scattered angle of 86.2° . While the results in Fig. 5 bear little resemblance to the data, those in Fig. 6 reproduce all the principal features. The reader should note the error bars included in our Fig. 7. There are uncertainties the order of 0.02 \AA in the data. The data at $E_I = 16 \text{ eV}$ and $\theta_s = 60^\circ$ do not extend far enough to positive values of Q_{\parallel} to see whether the cross section has the maximum indicated by theory. It is also the case that while the general shape of

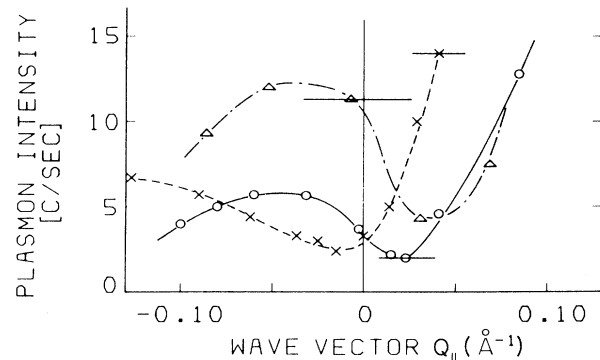


FIG. 7. The experimental data of Rocca and Valbusa, on the variation of the surface-plasmon excitation cross section with wave-vector transfer. The convention is the same as that used in Figs. 5 and 6. The figure has been reproduced from Figs. 3(a) of Ref. 4.

the other two curves agrees nicely with experiment, the theory places the minimum in the excitation cross section at values of Q_{\parallel} that are larger than found in the experiment.

As we have tried to outline during the course of our discussion, while our calculations of the surface-plasmon excitation cross section contain no adjustable parameters, once we have arrived at the image barrier used to generate the amplitudes R_s and R_I there are various approximations we have had to introduce at various stages. We are very pleased with the agreement between theory and experiment. Our conclusion is that the theory of dipole excitation put forth some years ago provides an adequate account of the excitation process, including the interference between the "loss then reflection," and "reflection

then loss" contributions to the matrix element. Under the conditions of the experiment reported by Rocca and his colleagues, this is controlled by the relative phase of R_I and R_s as well as their magnitude. Of course, the phase of the elastic scattering amplitude is not probed in LEED measurements.

ACKNOWLEDGMENTS

We are most grateful to Dr. Mario Rocca for supplying us with unpublished data on the LEED intensities for Ag(100), and for several useful discussions and comments. The research was supported by the U.S. Department of Energy, through Grant No. DE-FG03-84ER45083.

¹K. D. Tsuei, E. W. Plummer, and P. J. Feibelman, *Phys. Rev. Lett.* **63**, 2256 (1989).

²S. Suto, K. D. Tsuei, E. W. Plummer, and E. Burstein, *Phys. Rev. Lett.* **63**, 2590 (1989).

³K. D. Tsuei, E. W. Plummer, A. Liebsch, K. Kempa, and P. Bakshu, *Phys. Rev. Lett.* **64**, 44 (1989).

⁴M. Rocca and U. Valbusa, *Phys. Rev. Lett.* **64**, 2398 (1990).

⁵M. Rocca, F. Biggio, and U. Valbusa, *Phys. Rev. B* **42**, 2835 (1990).

⁶A. Eguiluz and J. J. Quinn, *Phys. Lett.* **53A**, 151 (1973); *Phys. Rev. B* **14**, 1347 (1976).

⁷J. O. Porteus and W. N. Faith, *Phys. Rev. B* **8**, 491 (1973).

⁸A. Bagchi and C. B. Duke, *Phys. Rev. B* **5**, 2784 (1972).

⁹C. B. Duke and U. Landman, *Phys. Rev. B* **8**, 505 (1973).

¹⁰B. N. J. Persson, *Solid State Commun.* **24**, 573 (1977).

¹¹D. L. Mills, *Surf. Sci.* **48**, 59 (1975). The content of this theory, along with several applications, are reviewed and discussed in Chapter 3 of H. Ibach and D. L. Mills, *Electron Energy Loss Spectroscopy and Surface Vibrations* (Academic, New York, 1982).

¹²See, for example, the discussion which precedes Eq. (4.3) of the paper cited in Ref. 11.

¹³E. Evans and D. L. Mills, *Phys. Rev. B* **5**, 4126 (1972); **7**, 853 (1973).

¹⁴H. Froitzheim and U. Kohler, *Phys. Rev. B* **40**, 8213 (1989).

¹⁵B. M. Hall, S. Y. Tong, and D. L. Mills, *Phys. Rev. Lett.* **50**, 1277 (1983).

¹⁶D. L. Mills, *Prog. Surf. Sci.* **8**, 143 (1977).

¹⁷M. Rocca (private communication).

¹⁸A. A. Lucas and M. Šunjić, *Phys. Rev. Lett.* **26**, 229 (1971).

¹⁹M. A. Van Hove and S. Y. Tong, *Surface Crystallography by LEED* (Springer-Verlag, Heidelberg, 1979).

²⁰E. Zanazzi, F. Jona, D. W. Jepsen, and P. M. Marcus, *J. Phys. C* **10**, 375 (1977).

²¹J. B. Pendry, *Low Energy Electron Diffraction* (Academic, New York, 1974).

²²A. G. Eguiluz (unpublished).

²³G. Malström and J. Rundgren, *Comput. Phys. Commun.* **19**, 263 (1980).

²⁴Burl M. Hall, Ph.D. thesis, University of Wisconsin-Milwaukee, 1983 (unpublished).

²⁵See the discussion given on pages 215 and 216 of Ref. 24.

²⁶E. G. McRae, *Rev. Mod. Phys.* **51**, 541 (1979); see the discussion in Sec. IV B 2.